

Low-Cost Exoskeletons for Learning Whole-Arm Manipulation in the Wild

Anonymous Author(s)

Affiliation

Address

email

Abstract: While humans can use parts of their arms other than the hands for manipulations like gathering and supporting, whether robots can effectively learn and perform the same type of operations remains relatively unexplored. As these manipulations require joint-level control to regulate the complete poses of the robots, we develop *AirExo*, a low-cost, adaptable, and portable dual-arm exoskeleton, for teleoperation and demonstration collection. As collecting teleoperated data is expensive and time-consuming, we further leverage *AirExo* to collect cheap in-the-wild demonstrations at scale. Under our in-the-wild learning framework, we show that with only 3 minutes of the teleoperated demonstrations, augmented by diverse and extensive in-the-wild data collected by *AirExo*, robots can learn a policy that is comparable to or even better than one learned from teleoperated demonstrations lasting over 20 minutes. Experiments demonstrate that our approach enables the model to learn a more general and robust policy across the various stages of the task, enhancing the success rates in task completion even with the presence of disturbances.

Keywords: AirExo, In-the-Wild Learning, Data Collection

1 Introduction

Robotic manipulation has emerged as a crucial field within the robot learning community and attracted significant attention from researchers. With the advancement of technologies such as deep learning, robotic manipulation has evolved beyond conventional grasping [9, 11, 33] and pick-and-place tasks [32, 43], encompassing a diverse array of complex and intricate operations [2, 3, 6, 10].

Most of the current robotic manipulation research focuses on interacting with the environment solely with the end-effectors of the robots, which correspond to the hands of human beings. However, as humans, we can also use other parts of our arms to accomplish or assist with various tasks in daily life. For example, holding objects with lower arms, closing fridge door with elbow, *etc.* In this paper, we aim to investigate and explore the ability of robots to effectively execute such tasks. To distinguish from the classical manipulation involving end-

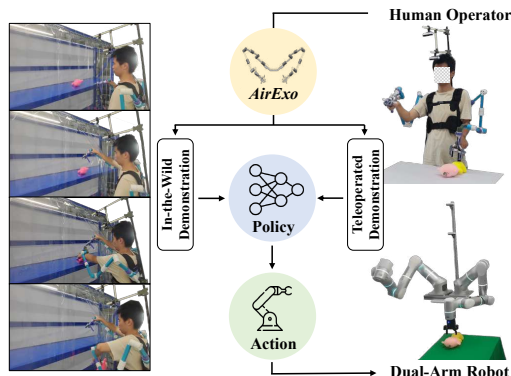


Figure 1: The methodology of our in-the-wild learning framework with low-cost exoskeletons *AirExo*. It empowers the human operator to not only control the dual-arm robots for collecting teleoperated demonstrations but also directly record in-the-wild demonstrations. Besides commonly-used teleoperated demonstrations, our learning framework also leverages the extensive and cheap in-the-wild demonstrations in policy learning, resulting in a more general and robust policy compared to training with even more teleoperated demonstrations.

39 effectors, we refer to these actions as **whole-arm manipulation**. Since most whole-arm manipula-
40 tion tasks require the coordinated collaboration of both limbs, we formalize them into the framework
41 of the bimanual manipulation problem.

42 While whole-arm manipulation is natural and simple for humans, it can become challenging for
43 robots. First, whole-arm manipulation usually implies extensive contact with the surrounding en-
44 vironment and collision risks during manipulation. Second, whole-arm manipulation necessitates
45 precise movement of the entire robot pose, as opposed to the conventional methods of only reaching
46 the end-effector pose at the destination. An intuitive approach to address these two challenges is to
47 adapt joint-level control for robots. To enable that, we adopt a joint-level imitation learning schema,
48 wherein joint-level control is needed when collecting the robot demonstration.

49 Recently, Zhao *et al.* [46] introduced an open-source low-cost ALOHA system which exhibits the
50 capability to perform joint-level imitation learning through real-world teleoperated data. ALOHA
51 system leverages two small, simple and modular bimanual robots ViperX [37] and WidowX [40]
52 that are almost identical to each other, to establish a leader-follower framework for teleoperation.
53 Due to the limited payload of the robots, they focus more on fine-grained manipulation. Besides,
54 their hardwares cannot be seamlessly adapted to other robots commonly employed for laboratory
55 research or industrial purposes. Similarly, while several literatures [8, 15, 17, 19, 45] also designed
56 special exoskeletons for certain humanoid robots or robot arms, the cross-robot transferability of
57 their exoskeletons remain a challenge.

58 To address the above issues, we develop *AirExo*, an *open-source, low-cost, robust* and *portable* dual-
59 arm exoskeleton system that can be quickly modified for different robots. All structural components
60 of *AirExo* are *universal* across robots and can be fabricated entirely through 3D printing, enabling
61 easy assembly even for non-experts. After calibration with a dual-arm robot, *AirExo* can achieve
62 precise joint-level teleoperations of the robot.

63 Contributed to its portable property, *AirExo* enables *in-the-wild data collection for dexterous ma-*
64 *nipulation without needing a robot*. Humans can wear the dual-arm exoskeleton system, conduct
65 manipulation in the wild, and collect demonstrations at scale. This breakthrough capability not only
66 simplifies data collection but also extends the reach of whole-arm manipulation into unstructured
67 environments, where robots can learn and adapt from human interactions. The one-to-one mapping
68 of joint configurations also reduces the barriers of transferring policies trained on human-collected
69 data to robots. Experiments show that with our in-the-wild learning framework, the policy can be-
70 come more sample efficient for the expensive teleoperated demonstrations, and can acquire more
71 high-level knowledge for task execution, resulting in a more general and robust strategy. The source
72 code, data and exoskeleton models will be made publicly available.

73 2 Related Works

74 **Imitation Learning** Imitation learning has been widely applied in robot learning to teach robots
75 how to perform various tasks by observing and imitating demonstrations from human experts. One
76 of the simplest methods in imitation learning is behavioral cloning [27], which learns the policy
77 directly in a supervised manner without considering intentions and outcomes. Most approaches
78 parameterize the policy using neural networks [2, 5, 31, 44, 46], while non-parametric VINN [26]
79 leverages the weighted k -nearest-neighbors algorithm based on the visual representations extracted
80 by BYOL [14] to generate the action from the demonstration database. This simple but effective
81 method can also be extended to other visual representations [22, 23, 25, 29] for robot learning. In
82 the context of imitation learning for bimanual manipulation, Xie *et al.* [41] introduced a paradigm to
83 decouple the high-level planning model into the elemental movement primitives. Several literature
84 have focused on designing special frameworks to solve specific tasks, such as knot tying [18, 34],
85 banana peeling [17], culinary activities [21], and fabric folding [39]. Addressing the challenge of
86 non-Markovian behavior observed in demonstrations, Zhao *et al.* [46] utilized the notion of action
87 chunking as a strategy to enhance overall performance.

88 **Teleoperation** Demonstration data play a significant role in robotic manipulation, particularly in
 89 the methods based on imitation learning. For the convenience of subsequent robot learning, these
 90 demonstration data are typically collected within the robot domain. A natural approach to gather
 91 such demonstrations is human teleoperation [24], where a human operator remotely controls the
 92 robot to execute various tasks. Teleoperation methods can be broadly categorized into two classes
 93 based on their control objectives: one aimed at manipulating the end-effectors of the robots [2, 7,
 94 10, 16, 30, 44] and one focused on regulating the complete poses of the entire robots, such as ex-
 95 oskeletons [8, 15, 17, 35, 45] and a pair of leader-follower robots [46]. For whole-arm manipulation
 96 tasks, we need to control the full pose of the robots, which makes exoskeletons a relatively favorable
 97 option under this circumstance.

98 **Learning Manipulation in the Wild** Despite the aforementioned teleoperation methods allow us
 99 to collect robotic manipulation data, the robot system is usually expensive and not portable, posing
 100 challenges to collect demonstration data at scale. To address this issue, previous research has ex-
 101 plored the feasibility of learning from interactive human demonstrations, *i.e.* in-the-wild learning
 102 for robotic manipulation [1, 4, 19, 28, 33, 42]. In contrast to the costly robot demonstrations, in-the-
 103 wild demonstrations are typically cheap and easy to obtain, allowing us to collect a large volume
 104 of such demonstrations conveniently. Typically, there are two primary domain gaps for learning
 105 manipulation in the wild: (1) the gap between human-operated images and robot-operated images,
 106 and (2) the gap between human kinematics and robot kinematics. The former gap can be solved
 107 through several approaches: by utilizing specialized end-effectors that match the end-effectors of the
 108 robots [19, 42]; by initially pre-training with in-the-wild data and subsequently fine-tuning with
 109 robot data [33]; or by applying special image processing technique to generate agent-agnostic im-
 110 ages [1]. The latter gap is currently addressed by applying structure from motion algorithms [33,
 111 42], adopting a motion tracking system [28], or training a pose detector [1, 38] to extract the desired
 112 poses. However, these methods are not suitable for whole-arm dexterous manipulation, since motion
 113 tracking usually focuses on the end-effector, and pose detector is vulnerable to visual occlusions and
 114 does not map to the robot kinematics.

115 3 AirExo: An Open-Source, Portable, Adaptable, Inexpensive and Robust 116 Exoskeleton

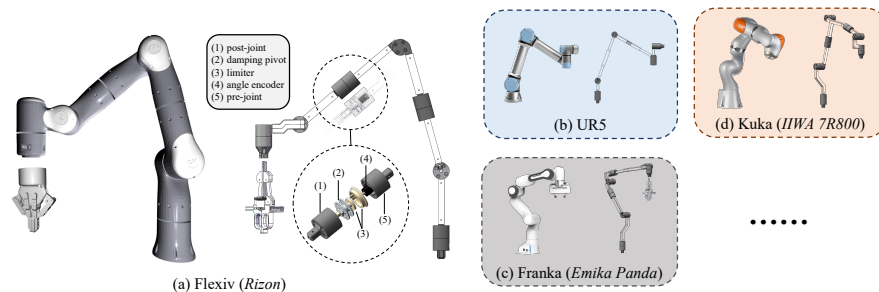


Figure 2: *AirExo* models for different types of robots. Notice that the internal structure of the joints is standardized, only the linkages are altered to accommodate different robotic arm configurations.

117 3.1 Exoskeleton

118 From the preceding discussions in Sec. 1, we summarize the following 5 key design objectives of an
 119 exoskeleton: (1) affordability; (2) adaptability; (3) portability; (4) robustness and (5) maintenance
 120 simplicity. Based on these design objectives, we develop *AirExo* as follows.

121 In this paper, we employ two Flexiv Rizon arms [12] for experiments. As a result, the structural
 122 design of *AirExo* is predominantly tailored to their specifications. Meanwhile, to ensure its uni-
 123 versality, it can be easily modified for use with other robotic arms like UR5 [36], Franka [13] and

124 Kuka [20], as depicted in Fig. 2. Based on the morphology of our robot system, *AirExo* is composed
 125 of two symmetrical arms, wherein the initial 7 degree-of-freedoms (DoFs) of each arm correspond
 126 to the DoFs of the robotic arm, and the last DoF corresponds to the end-effector of the robotic arm.
 127 Here, we design a two-finger gripper with 1 DoF as an optional end-effector for each arm. Overall,
 128 *AirExo* is capable of simulating the kinematics of the robot across its entire workspace, as well as
 129 emulating the opening and closing actions of the end-effectors.

130 According to design objective (3), to improve the wearable experience for operators and concurrently
 131 enhance task execution efficiency, we dimension *AirExo* to be 80% of the robot’s size, based on the
 132 length of the human arm. In the end-effector of the exoskeleton, we design a handle and a scissor-like
 133 opening-closing mechanism to simulate the function of a two-fingered gripper, while also facilitating
 134 gripping actions by the operator. The two arms of the exoskeleton are affixed to a base, which is
 135 mounted on a vest. This allows the operator to wear it stably, and evenly distributing the weight
 136 of the exoskeleton across the back of the operator to reduce the load on the arms, thereby enabling
 137 more flexible arm motions. Additionally, an adjustable camera mount can be installed on the base
 138 for image data collection during operations.

139 The joints of *AirExo* adapt a dual-layer structure, with the outer case divided into two parts: the
 140 portion proximate to the base is referred to as the *pre-joint*, while the other half is called the *post-*
 141 *joint*. As illustrated in Fig. 2(a), these two components are connected via a metal *damping pivot*, and
 142 their outer sides are directly linked to the connecting rod. *AirExo* primarily achieves high-precision
 143 and low-latency motion capture through the *angle encoders* (with a resolution of 0.08 degrees),
 144 whose bases are affixed to the *pre-joints*. The pivots of the encoders are connected to the *post-joint*
 145 through a *limiter*, which is comprised of a dual-layer disc and several steel balls to set the angle limit
 146 for each joint. The dual-layer joint structure ensures that the encoders remain unaffected by bending
 147 moments during motions, rotating synchronously with the joints, which safeguards the encoders and
 148 reduces failures effectively. This aligns with the design objective (4) and (5).

149 Except the fasteners, damping pivots, and electronic components, all other components of *AirExo* are
 150 fabricated using PLA plastic through 3D printing. The material has a high strength and a low density,
 151 thereby achieving a lightweight but robust exoskeleton. The prevalence of 3D-printed components
 152 allows the exoskeleton to be easily adapted to different robots. This adaptation entails adjusting
 153 the dimensions of certain components based on the target robot’s specifications and subsequently
 154 reprinting and installing them, without modifying the internal structure. *AirExo* costs approximately
 155 \$600 in total, which is in accordance with the design objective (1).

156 3.2 Calibration and Teleoperation

157 Since *AirExo* shares the same morphology with the dual-arm robot except for the scale, the calibra-
 158 tion process can be performed in a quite straightforward manner. After positioning the robot arms
 159 at a specific location like a fully extended position, and aligning the exoskeleton to match the robot
 160 posture, we can record the joint positions $\{q_i^{(c)}\}_{i=1}^d$ and the encoder readings $\{p_i^{(c)}\}_{i=1}^d$ of *AirExo*,
 161 where d denotes the DoFs. Consequently, during teleoperation, we only need to fetch the encoder
 162 readings $\{p_i\}_{i=1}^d$ and transform them into the corresponding joint positions $\{q_i\}_{i=1}^d$ using Eqn. (1),
 163 and let the robot moves to the desired joint positions:

$$q_i = \min \left(\max \left(q_i^{(c)} + k_i(p_i - p_i^{(c)}), q_i^{\min} \right), q_i^{\max} \right), \quad (1)$$

164 where $k_i \in \mathbb{R}$ is the coefficient controlling direction and scale, and q_i^{\min}, q_i^{\max} denote the joint angle
 165 limits of the robotic arms. Typically, we set $k = \pm 1$, representing the consistency between the
 166 encoder direction of the exoskeleton and the joint direction of the robot. For grippers, we can
 167 directly map the angle range of the encoders to the opening and closing range of the grippers for
 168 teleoperation.

169 After calibration, the majority of angles within the valid range of the robot arms can be covered by
 170 the exoskeleton. Given that the workspaces of most tasks fall within this coverage range, we can
 171 teleoperate the robot using the exoskeleton conveniently and intuitively. If a special task t needs a

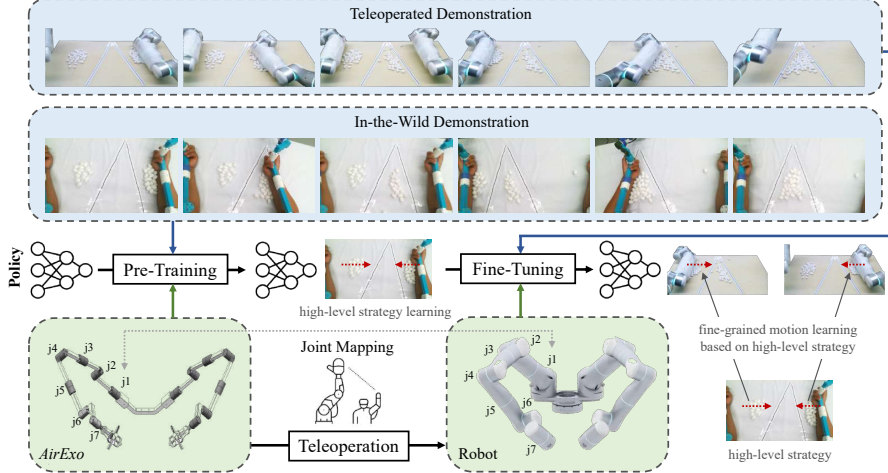


Figure 3: Overview of learning whole-arm manipulations in the wild with *AirExo*. First, we use in-the-wild demonstrations and exoskeleton actions that are transformed into the robot’s domain to pre-train the policy, which corresponds to learning the high-level strategy of task execution. Then, we use teleoperated demonstrations and robot actions to fine-tune the policy, which corresponds to learning fine-grained motion based on the learned high-level strategy.

172 wider operation range, we can simply scale the exoskeleton range using coefficients k_i , and apply
 173 task-specific joint constraint $[q_i^{l,\min}, q_i^{l,\max}]$ instead of original kinematic constraint in Eqn. (1) for
 174 better teleoperation performance.

175 3.3 In-the-Wild Learning with AirExo

176 For in-the-wild whole-arm manipulation learning, we install a camera (or cameras under multi-
 177 camera settings) on the camera mount of *AirExo* in roughly the same position(s) as the camera(s) on
 178 the robot. Using this configuration, images from both teleoperated demonstrations and in-the-wild
 179 demonstrations exhibit a relatively similar structure, which is advantageous for policy learning.

180 Our approach to learn whole-arm manipulation in the wild with *AirExo* is illustrated in Fig. 3. As
 181 we discussed in Sec. 2, *AirExo* serves as a natural bridge for the kinematic gap between humans and
 182 robots. To address the domain gap between images, our approach involves a two-stage training pro-
 183 cess. In the first stage, we pre-train the policy using in-the-wild human demonstrations and actions
 184 recorded by the exoskeleton encoders. During this phase, the policy primarily learns the high-level
 185 task execution strategy from the large-scale and diverse in-the-wild human demonstrations. Sub-
 186 sequently, in the second stage, the policy undergoes fine-tuning using teleoperated demonstrations
 187 with robot actions to refine the motions based on the previously acquired high-level task execution
 188 strategy.

189 As previously discussed in Sec. 3.1, we resize the exoskeleton to ensure its wearability. Some con-
 190 cerns may arise regarding whether this scaling adjustment could impact the policy learning process.
 191 Here, we argue that it has a minimal effect on our learning procedure. Firstly, the core kinematic
 192 structure, essential for our learning framework, remain unaffected by the resizing. Thus human
 193 demonstrations preserve the fundamental dynamics of the system. Secondly, our approach does not
 194 impose strict alignment requirements between human demonstration images and robot images. We
 195 find that similar visual-action pairs collected by our exoskeleton effectively support the pretraining
 196 stage, without demanding precise visual matching between human and robot demonstrations.

197 We use the state-of-the-art bimanual imitation learning method ACT [46] for policy learning. Our
 198 experiments demonstrate that it can indeed learn the high-level strategy through the pre-training
 199 process and significantly enhance the evaluation performance of the robot and the sample efficiency
 200 of the expensive teleoperated demonstrations.

201 **4 Experiments**

202 In this section, we conduct experiments on 2 whole-arm tasks to evaluate the performance of the
203 proposed learning method. All demonstration data are collected by *AirExo*.

204 **4.1 Gather Balls: Setup**

205 **Task** Two clusters of cotton balls are randomly placed on both sides of the tabletop (40 balls per
206 cluster). The goal is to gather these balls into the designated central triangular area using both arms.
207 The process of this contact-rich task is illustrated in Fig. 4.

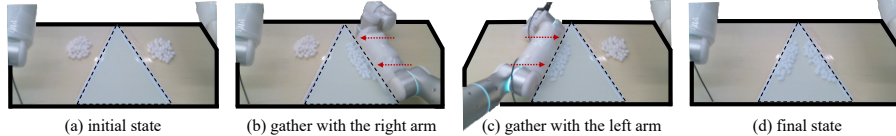


Figure 4: Definition of *Gather Balls* task. The goal is to gather the balls into the central triangular area, which is highlighted in light blue. The red dashed arrows denote the motions of the robot arms. Sponge paddings are used to envelop the external surface of the robot arms to diminish the mechanical failures arising from contacts.

208 **Metrics** We consider the percentage of balls being allocated within the central triangular area as
209 the task completion rate c (if a ball is precisely on the line, it is considered a half), including both the
210 completion rates of the left arm and the right arm. Simultaneously, task success is defined as the task
211 completion rate exceeding a certain threshold δ . In this experiment, we set $\delta = 40\%, 60\%, 80\%$. We
212 also record the collision rate to gauge the precision of the operations.

213 **Methods** We employ VINN [26] and its variants that alter the visual representations [22, 23, 29]
214 as non-parametric methods. Other methods include ConvMLP [44], BeT [31] and ACT [46]. All
215 of them are designed for joint-space control or can be easily adapted for joint-space control. We
216 apply our proposed learning approach to ACT for learning from in-the-wild demonstrations. For all
217 methods, we carefully select the hyper-parameters to ensure better performance.

218 **Protocols** The evaluation is conducted on a workstation equipped with an Intel Core i9-10980XE
219 CPU. The time limit is set as 60 seconds per trial. Given that all methods can operate at approxi-
220 mately 5Hz, resulting in a total of 300 steps for the evaluation, the time constraint proves sufficient
221 for the task. We conduct 50 consecutive trials to ensure stable and accurate results, calculating the
222 aforementioned metrics.

223 **4.2 Gather Balls: Results and Analyses**

224 The experimental results on the *Gather Balls* task are shown in Tab. 1. When using 50 teleoperated
225 demonstrations as training data, VINN performs the best among all non-parametric methods, while
226 ACT excels among all parametric methods. When using only 10 teleoperated demonstrations for
227 training, the performance of both VINN and ACT degrades inevitably. However, after applying
228 our in-the-wild learning framework, with the assistance of in-the-wild demonstrations, ACT can
229 achieve the same level of performance as 50 teleoperated demonstrations with just 10 teleoperated
230 demonstrations. This demonstrates that our learning framework with in-the-wild demonstrations
231 makes the policy more sample-efficient for teleoperated demonstrations.

232 We then delve into the experimental results to provide more insights about why and how our learning
233 framework works. When analyzing the failure cases of different methods in the experiments in
234 Fig. 5(a), we find that the ACT policy trained solely on teleoperated demonstrations exhibits an
235 issue of imbalance between accuracies of two arms, with better learning outcomes for the left arm.
236 This imbalance becomes more pronounced as the number of teleoperated demonstrations decreases
237 to 10. With the help of the in-the-wild learning stage, the policy becomes more balanced between

# Demos		Method	Completion Rate c (%) \uparrow			Success Rate (%) \uparrow		
Teleop.	i.t.w		Overall	Left	Right	$c \geq 80$	$c \geq 60$	$c \geq 40$
50	-	VIP [22] + NN	27.74	0.02	55.45	0	0	36
50	-	VC-1 [23] + NN	52.54	32.53	72.55	4	42	74
50	-	MVP [29] + NN	55.10	58.55	62.00	12	62	76
50	-	VINN [26]	76.88	75.73	78.03	58	84	94
50	-	ConvMLP [44]	15.56	2.35	28.78	0	0	2
50	-	BeT [31]	24.66	7.38	41.95	0	2	32
50	-	ACT [46]	75.61	94.63	56.60	54	70	100
10	-	VINN [26]	68.68	60.28	77.08	36	76	88
10	-	ACT [46]	64.31	91.95	36.68	24	60	96
10	50	ACT [46]	73.76	88.83	58.70	62	72	88
10	100	ACT [46]	75.15	75.63	74.68	56	80	88

Table 1: Experimental results on the *Gather Balls* task. Here “teleop.” denotes teleoperated demonstrations and “i.t.w.” denotes in-the-wild demonstrations.

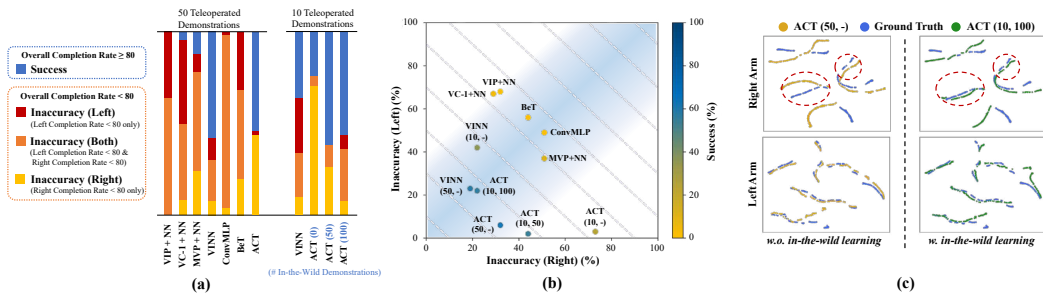


Figure 5: Analyses of methods on the *Gather Balls* task. Here we define the overall completion rate over 80% as success. (a) We analyze the failure causes of each method in every trial. (b) We amortize the inaccuracy (both) rate evenly into the inaccuracy (left) and inaccuracy (right) rates, and draw a comparison plot of failure modes for different methods. (x, y) means the policy is trained with y in-the-wild demonstrations then x teleoperated demonstrations. The dashed lines represent contour lines with the same success rate, and the regions with light blue background imply a more balanced policy between left and right arms. (c) t -SNE visualizations of the ground-truth actions and the policy actions w/o in-the-wild learning on the validation set.

238 two arms even with fewer teleoperated demonstrations, as shown in Fig. 5(b). From Fig. 5(c), we
 239 also observe that the policy focuses more on learning the motions of the right arm when cooperated
 240 with in-the-wild learning, as highlighted in red dashed circles, while keeping the accurate action
 241 predictions on the left arm. We believe that this is attributed to the extensive, diverse, and accurate
 242 in-the-wild demonstrations provided by *AirExo*, enabling the policy to acquire high-level strategy
 243 knowledge during the pre-training stage. Consequently, in the following fine-tuning stage, it can
 244 refine its actions based on the strategy, thus avoiding learning actions blindly from scratch.

245 4.3 Grasp from the Curtained Shelf: Setup and Results

246 **Task** A cotton toy is randomly placed in the center of a shelf with curtains. The goal is to grasp
 247 the toy and throw it into a bin. To achieve it, the robot needs to use its right arm to push aside the
 248 transparent curtain first, and maintain this pose during the following operations. The process of this
 249 multi-stage task is illustrated in Fig. 6.

250 **Metrics, Methods, and Protocols** We calculate the average success rate at the end of each stage
 251 as metrics. Based on the experimental results on the *Gather Balls* task, we select VINN [26] and
 252 ACT [46] as methods in experiments, as well as ACT equipped with our in-the-wild learning frame-
 253 work. The evaluation protocols are the same as the *Gather Balls* task, except that the time limit is
 254 120 seconds (about 400 steps) and the number of trials is 25.

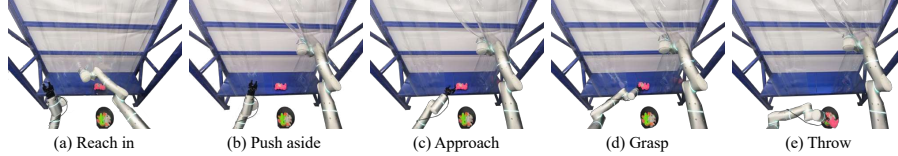


Figure 6: Definition of the *Grasp from the Curtained Shelf* task. The robot needs to (a) reach in its right arm to the transparent curtain and (b) push aside the curtain, then (c) approach the object with its left arm, (d) grasp the object and finally (e) throw the object.

255 **Results** The results are
 256 given in Tab. 2. Similar
 257 to the results of the *Gather*
 258 *Balls* task, as the num-
 259 ber of training teleoperated
 260 demonstrations is reduced,
 261 both VINN and ACT ex-
 262 perience a decrease in suc-
 263 cess rates, especially in the
 264 later “throw” stage. How-
 265 ever, after training with our
 266 in-the-wild learning framework, ACT exhibits a significant improvement in success rates in the
 267 “grasp” and “throw” stages. It achieves even higher success rates, surpassing those obtained with
 268 the original set of 50 teleoperated demonstrations lasting more than 20 minutes, using only 10 such
 269 demonstrations lasting approximately 3 minutes. This highlights that our proposed in-the-wild
 270 framework indeed enables the policy to learn a better strategy, effectively enhancing the success
 271 rates in the later stages of multi-stage tasks.

# Demos	i.t.w.	Method	Success Rate (%) ↑				
			Reach in	Push aside	Approach	Grasp	Throw
50	-	VINN [26]	100	96	92	60	48
50	-	ACT [46]	100	100	100	84	84
10	-	VINN [26]	100	84	84	60	44
10	-	ACT [46]	100	100	96	72	44
10	50	ACT [46]	100	100	96	76	76
10	100	ACT [46]	100	100	100	92	88

Table 2: Experimental results on the *Grasp from the Curtained Shelf* task.

272 **Robustness Analysis** We design three kinds
 273 of disturbances in the robustness experiments
 274 to explore whether in-the-wild learning im-
 275 proves the robustness of the policy. The results
 276 shown in Tab. 3 demonstrate that our in-the-
 277 wild learning framework can leverage diverse
 278 in-the-wild demonstrations to make the learned
 279 policy more robust and generalizable to various
 280 environmental disturbances.

Disturbances w/wo i.t.w. learning	Success / All
Novel Object	✗ / 8
	✓ / 8
Different Background	✗ / 8
	✓ / 8
Visual Distractors	✗ / 8
	✓ / 8

Table 3: Results of the robustness experiments on the *Grasp from the Curtained Shelf* task.

281 5 Conclusion

282 In this paper, we develop *AirExo*, an open-source, low-cost, universal, portable, and robust exoskele-
 283 ton, for both joint-level teleoperation of the dual-arm robot and learning whole-arm manipulations
 284 in the wild. Our proposed in-the-wild learning framework decreases the demand for the resource-
 285 intensive teleoperated demonstrations. Experimental results show that policies learned through this
 286 approach gain a high-level understanding of task execution, leading to improved performance in
 287 multi-stage whole-arm manipulation tasks. This outperforms policies trained from scratch using
 288 even more teleoperated demonstrations. Furthermore, policies trained in this framework exhibit
 289 increased robustness in the presence of various disturbances.

290 In the future, we are excited to see our *AirExo* collecting large-scale demonstrations in unstructured
 291 environments and facilitating robot learning. We will investigate how to better address the image
 292 gap between in-the-wild data in the human domain and teleoperated data in the robot domain, en-
 293 abling robots to learn solely through large-scale in-the-wild demonstrations with *AirExo*, thus further
 294 reducing the learning cost.

References

- 296 [1] Shikhar Bahl, Abhinav Gupta, and Deepak Pathak. “Human-to-Robot Imitation in the Wild”. In:
297 *Robotics: Science and Systems (RSS)*. 2022.
- 298 [2] Anthony Brohan et al. “RT-1: Robotics Transformer for Real-World Control at Scale”. In: *Robotics:
299 Science and Systems (RSS)*. 2023.
- 300 [3] Anthony Brohan et al. “RT-2: Vision-Language-Action Models Transfer Web Knowledge to Robotic
301 Control”. In: *arXiv preprint arXiv:2307.15818* (2023).
- 302 [4] Annie S. Chen, Suraj Nair, and Chelsea Finn. “Learning Generalizable Robotic Reward Functions from
303 ”In-The-Wild” Human Videos”. In: *Robotics: Science and Systems (RSS)*. 2021.
- 304 [5] Cheng Chi et al. “Diffusion Policy: Visuomotor Policy Learning via Action Diffusion”. In: *Robotics:
305 Science and Systems (RSS)*. 2023.
- 306 [6] Danny Driess et al. “PaLM-E: An Embodied Multimodal Language Model”. In: *International Confer-
307 ence on Machine Learning (ICML)*. Vol. 202. PMLR, 2023, pp. 8469–8488.
- 308 [7] Frederik Ebert et al. “Bridge Data: Boosting Generalization of Robotic Skills with Cross-Domain
309 Datasets”. In: *Robotics: Science and Systems (RSS)*. 2022.
- 310 [8] Fabian Falck, Kawin Larppichet, and Petar Kormushev. “DE VITO: A Dual-Arm, High Degree-of-
311 Freedom, Lightweight, Inexpensive, Passive Upper-Limb Exoskeleton for Robot Teleoperation”. In:
312 *Towards Autonomous Robotic Systems: 20th Annual Conference, TAROS 2019, London, UK, July 3–
313 5, 2019, Proceedings, Part I 20*. Springer. 2019, pp. 78–89.
- 314 [9] Hao-Shu Fang et al. “AnyGrasp: Robust and Efficient Grasp Perception in Spatial and Temporal Do-
315 mains”. In: *IEEE Transactions on Robotics (TRO)* (2023).
- 316 [10] Hao-Shu Fang et al. “RH20T: A Robotic Dataset for Learning Diverse Skills in One-Shot”. In: *RSS 2023
317 Workshop on Learning for Task and Motion Planning*. 2023.
- 318 [11] Hao-Shu Fang et al. “Robust Grasping across Diverse Sensor Qualities: The GraspNet-1Billion Dataset”.
319 In: *The International Journal of Robotics Research* (2023), p. 02783649231193710.
- 320 [12] *Flexiv Rizon Robot*. URL: <https://www.flexiv.com/en/technology/robot>.
- 321 [13] *Franka Emika Panda*. URL: <https://www.franka.de/research>.
- 322 [14] Jean-Bastien Grill et al. “Bootstrap Your Own Latent - A New Approach to Self-Supervised Learning”.
323 In: *Advances in Neural Information Processing Systems (NeurIPS)*. Vol. 33. 2020, pp. 21271–21284.
- 324 [15] Yasuhiro Ishiguro et al. “Bilateral Humanoid Teleoperation System Using Whole-Body Exoskeleton
325 Cockpit TABLIS”. In: *IEEE Robotics and Automation Letters* 5.4 (2020), pp. 6419–6426.
- 326 [16] Eric Jang et al. “BC-Z: Zero-Shot Task Generalization with Robotic Imitation Learning”. In: *Conference
327 on Robot Learning (CoRL)*. PMLR. 2021, pp. 991–1002.
- 328 [17] Heecheol Kim, Yoshiyuki Ohmura, and Yasuo Kuniyoshi. “Robot Peels Banana with Goal-Conditioned
329 Dual-Action Deep Imitation Learning”. In: *arXiv preprint arXiv:2203.09749* (2022).
- 330 [18] Heecheol Kim, Yoshiyuki Ohmura, and Yasuo Kuniyoshi. “Transformer-Based Deep Imitation Learning
331 for Dual-Arm Robot Manipulation”. In: *IEEE/RSJ International Conference on Intelligent Robots and
332 Systems (IROS)*. IEEE. 2021, pp. 8965–8972.
- 333 [19] Heecheol Kim et al. “Training Robots Without Robots: Deep Imitation Learning for Master-to-Robot
334 Policy Transfer”. In: *IEEE Robotics and Automation Letters* 8.5 (2023), pp. 2906–2913.
- 335 [20] *Kuka IIWA 7R800*. URL: [https://www.kuka.com/en-de/products/robot-systems/
336 industrial-robots/lbr-iiwa](https://www.kuka.com/en-de/products/robot-systems/industrial-robots/lbr-iiwa).
- 337 [21] Junjia Liu et al. “Robot Cooking with Stir-Fry: Bimanual Non-Prehensile Manipulation of Semi-Fluid
338 Objects”. In: *IEEE Robotics and Automation Letters* 7.2 (2022), pp. 5159–5166.
- 339 [22] Yecheng Jason Ma et al. “VIP: Towards Universal Visual Reward and Representation via Value-Implicit
340 Pre-Training”. In: *International Conference on Learning Representations (ICLR)*. 2023.
- 341 [23] Arjun Majumdar et al. “Where are We in the Search for an Artificial Visual Cortex for Embodied Intel-
342 ligence?” In: *ICRA 2023 Workshop on Pretraining for Robotics*. 2023.
- 343 [24] Ajay Mandlekar et al. “ROBOTURK: A Crowdsourcing Platform for Robotic Skill Learning through
344 Imitation”. In: *Conference on Robot Learning (CoRL)*. PMLR. 2018, pp. 879–893.
- 345 [25] Suraj Nair et al. “R3M: A Universal Visual Representation for Robot Manipulation”. In: *Conference on
346 Robot Learning (CoRL)*. PMLR. 2022, pp. 892–909.
- 347 [26] Jyothish Pari et al. “The Surprising Effectiveness of Representation Learning for Visual Imitation”. In:
348 *Robotics: Science and Systems (RSS)*. 2022.
- 349 [27] Dean A Pomerleau. “ALVINN: An Autonomous Land Vehicle in a Neural Network”. In: *Advances in
350 Neural Information Processing Systems (NeurIPS)*. Vol. 1. 1988.
- 351 [28] Pragathi Praveena et al. “Characterizing Input Methods for Human-to-Robot Demonstrations”. In:
352 *ACM/IEEE International Conference on Human-Robot Interaction (HRI)*. IEEE. 2019, pp. 344–353.

- 353 [29] Ilija Radosavovic et al. “Real-World Robot Learning with Masked Visual Pre-Training”. In: *Conference*
354 *on Robot Learning (CoRL)*. PMLR. 2022, pp. 416–426.
- 355 [30] Erick Rosete-Beas et al. “Latent Plans for Task Agnostic Offline Reinforcement Learning”. In: *Confer-*
356 *ence on Robot Learning (CoRL)*. PMLR. 2022, pp. 1838–1849.
- 357 [31] Nur Muhammad Shafiullah et al. “Behavior Transformers: Cloning k Modes with One Stone”. In: *Ad-*
358 *vances in Neural Information Processing Systems (NeurIPS)*. Vol. 35. 2022, pp. 22955–22968.
- 359 [32] Anthony Simeonov et al. “Neural Descriptor Fields: SE(3)-Equivariant Object Representations for
360 Manipulation”. In: *IEEE International Conference on Robotics and Automation (ICRA)*. IEEE. 2022,
361 pp. 6394–6400.
- 362 [33] Shuran Song et al. “Grasping in the Wild: Learning 6DoF Closed-Loop Grasping from Low-Cost
363 Demonstrations”. In: *IEEE Robotics and Automation Letters* 5.3 (2020), pp. 4978–4985.
- 364 [34] Kanata Suzuki et al. “In-Air Knotting of Rope Using Dual-Arm Robot Based on Deep Learning”. In:
365 *IEEE/RSJ International Conference on Intelligent Robots and Systems (IROS)*. IEEE. 2021, pp. 6724–
366 6731.
- 367 [35] Alexander Toedtheide et al. “A Force-Sensitive Exoskeleton for Teleoperation: An Application in El-
368 derly Care Robotics”. In: *IEEE International Conference on Robotics and Automation (ICRA)*. IEEE.
369 2023, pp. 12624–12630.
- 370 [36] *UR5 Robot*. URL: <https://www.universal-robots.com/products/ur5-robot>.
- 371 [37] *ViperX 300 Robot Arm 6DoF*. URL: [https://www.trossenrobotics.com/viperx-300-](https://www.trossenrobotics.com/viperx-300-robot-arm-6dof.aspx)
372 [robot-arm-6dof.aspx](https://www.trossenrobotics.com/viperx-300-robot-arm-6dof.aspx).
- 373 [38] Chen Wang et al. “MimicPlay: Long-Horizon Imitation Learning by Watching Human Play”. In: *arXiv*
374 *preprint arXiv:2302.12422* (2023).
- 375 [39] Thomas Weng et al. “FabricFlowNet: Bimanual Cloth Manipulation with a Flow-based Policy”. In:
376 *Conference on Robot Learning (CoRL)*. PMLR. 2021, pp. 192–202.
- 377 [40] *WidowX 250 Robot Arm 6DoF*. URL: [https://www.trossenrobotics.com/widowx-250-](https://www.trossenrobotics.com/widowx-250-robot-arm-6dof.aspx)
378 [robot-arm-6dof.aspx](https://www.trossenrobotics.com/widowx-250-robot-arm-6dof.aspx).
- 379 [41] Fan Xie et al. “Deep Imitation Learning for Bimanual Robotic Manipulation”. In: *Advances in Neural*
380 *Information Processing Systems (NeurIPS)*. Vol. 33. 2020, pp. 2327–2337.
- 381 [42] Sarah Young et al. “Visual Imitation Made Easy”. In: *Conference on Robot Learning (CoRL)*. PMLR.
382 2020, pp. 1992–2005.
- 383 [43] Andy Zeng et al. “Transporter Networks: Rearranging the Visual World for Robotic Manipulation”. In:
384 *Conference on Robot Learning (CoRL)*. PMLR. 2020, pp. 726–747.
- 385 [44] Tianhao Zhang et al. “Deep Imitation Learning for Complex Manipulation Tasks from Virtual Reality
386 Teleoperation”. In: *IEEE International Conference on Robotics and Automation (ICRA)*. IEEE. 2018,
387 pp. 5628–5635.
- 388 [45] Liang Zhao et al. “A Wearable Upper Limb Exoskeleton for Intuitive Teleoperation of Anthropomorphic
389 Manipulators”. In: *Machines* 11.4 (2023), p. 441.
- 390 [46] Tony Z Zhao et al. “Learning Fine-Grained Bimanual Manipulation with Low-Cost Hardware”. In:
391 *Robotics: Science and Systems (RSS)*. 2023.